

Article

Preparation and Mercury Removal Performance of Mg-MOF-74 Composites

Yue Yu ¹, Jizu Li ¹, Peng Cheng ², Haotian Nie ², Ling He ², Qizhen Yan ², Yulan Zheng ², Yawen Wu ² and Li Jia ^{2,*} 

¹ College of Economics and Management, Taiyuan University of Technology, Taiyuan 030024, China; yuyue@tyut.edu.cn (Y.Y.); lijizu@tyut.edu.cn (J.L.)

² College of Electrical and Power Engineering, Taiyuan University of Technology, Taiyuan 030024, China; 13955610472@163.com (P.C.); niehaotian0327@163.com (H.N.); hl2058313563@163.com (L.H.); 13835005456@163.com (Q.Y.); 13453602769@163.com (Y.Z.); 13111212809@163.com (Y.W.)

* Correspondence: jiali@tyut.edu.cn

Abstract: A metal–organic framework (MOF) material Mg-MOF-74 was prepared by a solvothermal method, and the influence of the solvent volume and mass–liquid ratio on the preparation process was investigated. Based on the iron-based modified biochar FeCeCu/BC obtained by the sol–gel method, functionalized modified MOF-based biochar composites were prepared by the physical mixing method, co-pyrolysis method, sol–gel method and in situ growth method. The mercury removal performance and structural characteristics of the samples were studied, and the adsorption mechanism and key action mechanism were studied by using the adsorption kinetic model. Increasing the solvent volume and the mass liquid ratio will make the crystallization and pore structure of Mg-MOF-74 worse and its mercury removal performance poor. For MOF-based FeCeCu/BC composites, the mercury removal performance of the composite samples prepared by the sol–gel method and co-pyrolysis method is the best, at 31% and 46% higher than that of modified biochar, respectively. Mg-MOF-74 plays a role in promoting pyrolysis and changing the pore structure in the composite. The mercury removal process of composite materials is the result of physical adsorption and chemical adsorption, external mass transfer and internal diffusion.

Keywords: Mg-MOF-74; biochar; composite; mercury removal



Citation: Yu, Y.; Li, J.; Cheng, P.; Nie, H.; He, L.; Yan, Q.; Zheng, Y.; Wu, Y.; Jia, L. Preparation and Mercury Removal Performance of Mg-MOF-74 Composites. *Atmosphere* **2023**, *14*, 1551. <https://doi.org/10.3390/atmos14101551>

Academic Editor: James Cizdziel

Received: 19 September 2023

Revised: 6 October 2023

Accepted: 9 October 2023

Published: 11 October 2023



Copyright: © 2023 by the authors. Licensee MDPI, Basel, Switzerland. This article is an open access article distributed under the terms and conditions of the Creative Commons Attribution (CC BY) license (<https://creativecommons.org/licenses/by/4.0/>).

1. Introduction

At present, mercury pollution caused by anthropogenic emissions has aroused widespread concern because of its great harm to human health. China is the largest emitter of anthropogenic mercury in the world, with more than 600 tons of annual mercury emissions, which contribute about 28% of total global anthropogenic emissions [1]. The mercury emitted by coal-fired power plants is the largest single source, accounting for more than one-third of the total anthropogenic mercury emissions, mainly including gaseous mercuric oxide (Hg²⁺), gaseous elemental mercury (Hg⁰) and particulate mercury (Hg^P) [2]. Most of the particulate mercury is oxidized mercury and elemental mercury attached to fly ash and residual carbon, which can be removed synergistically by the existing flue gas purification equipment, while most of the remaining elemental mercury and a small amount of oxidized mercury will be discharged into the atmosphere in a gaseous form. In 2014, China required the emission limit of mercury in the flue gas of coal-fired power plants to be 50 µg/m³ [3]. At the same time, with the introduction of the Minamata Convention on Mercury in 2017, the treatment of mercury pollutants in coal-fired power plants has become an urgent problem to be solved in the face of international compliance and emission reduction pressure. At present, it is generally agreed that the adsorbent injection process is the most promising method to control mercury emissions from coal-fired power plants, but the commonly used active carbon adsorbents have some disadvantages, such as high cost, poor reproducibility, narrow temperature range, competitive adsorption, etc. [4]. Therefore, it is necessary to

develop high-performance and low-cost mercury adsorbents in today's coal-fired power plants, which are already difficult to operate.

Studies have shown that materials such as fly ash, mineral substances and biochar can be used for mercury adsorption [5–7]. Jiali et al. [8] found that walnut shell biochar modified by metal doping has an abundant surface structure and functional groups, which makes it more effective for the removal of gaseous elemental mercury, and can be used as an alternative material for activated carbon mercury removal agents. Metal–organic frameworks (MOFs), a new type of porous crystal material, are mainly formed by the self-assembly of central metals and organic ligands. Due to their large specific surface area, abundant pores, adjustable size and other advantages, they have attracted wide attention in the fields of gas adsorption separation, biological medicine and other fields in recent years, especially for the adsorption of gaseous pollutants [9,10]. However, the practical application of pure MOF materials is limited by their high preparation cost and poor chemical stability. Organic ligands in MOF materials can be easily compounded with other materials for preparation, so researchers have gradually shifted their research focus to MOF composites.

Mg-MOF-74, also known as CPO-27-Mg, is a metal–organic framework material with a hexagon pore structure that is connected by Mg^{2+} and the organic bridging ligand 2,5-dihydroxyterephthalic acid (H_4DOBD C) [11,12], which has a high specific surface area and good thermal stability and has great potential in the field of gas adsorption, but research on mercury removal applications has not been widely carried out. At the same time, its surface contains a large number of functional groups, such as carboxyl and hydroxyl groups, from organic ligands, which provides favorable conditions for preparing composite materials.

In summary, in this paper, Mg-MOF-74 was prepared by a solvothermal method, and the influence of solvent volume and mass–liquid ratio on the preparation process was investigated. Based on walnut shell biochar doped with 10%Fe-4%Ce-2%Cu prepared by the sol–gel method, MOF-based modified biochar composites were prepared by the physical mixing method, co-pyrolysis method, sol–gel method and in situ growth method. The composite mechanism, structural characteristics and removal performance of elemental mercury of the composites were characterized and experimentally investigated. Key data and a theoretical basis were provided for obtaining high-performance and low-cost mercury adsorbents.

2. Materials and Methods

2.1. Reagents

Magnesium nitrate hexahydrate ($Mg(NO_3)_2 \cdot 6H_2O$, 99%); 2,5-dihydroxyterephthalic acid (H_4DOBD C, 98%); ferric chloride hexahydrate ($FeCl_3 \cdot 6H_2O$, AR); cerium (III) nitrate hexahydrate ($Ce(NO_3)_3 \cdot 6H_2O$, AR); cupric sulfate pentahydrate ($CuSO_4 \cdot 5H_2O$, AR); ethanol absolute (EtOH, AR); N,N-Dimethylformamide (DMF, AR); propylene oxide (AR); tetraethyl orthosilicate (AR); deionized water.

2.2. Characterization Instruments

XRD characterization was performed using an Empyrean series X-ray diffractometer (Panaco, Amsterdam, The Netherlands), with the test target being a copper target, with a scan rate of $10^\circ/\text{min}$; thermogravimetric testing was performed using a HCT-1 comprehensive thermal analyzer (Hengjiu, Beijing, China) with a temperature range of room temperature to 800°C and a set temperature rise rate of $10^\circ\text{C}/\text{min}$ under N_2 atmosphere; FT-IR characterization was performed using the Nicolet iS20 Fourier Transform Infrared Spectrometer (Thermo Fisher, Waltham, MA, USA), with 32 scanning times and a scanning range of $400\text{--}4000\text{ cm}^{-1}$; adsorption and desorption isotherms of the samples were obtained by performing N_2 adsorption and desorption experiments with an ASAP 2460 analyzer (Micromeritics, Norcross, GA, USA), the specific surface area was obtained from the Brunauer–Emmett–Teller (BET) equation, and the pore structure parameters of the samples were obtained by the Barrett–Joyner–Halenda (BJH) and t-plot methods; microscopic

morphology of sample was obtained using a JSM-7900F SEM device (JEOL, Tokyo, Japan) operated at 10 kV.

2.3. Test System

A self-designed fixed-bed biochar preparation test system was used to conduct the 600 °C pyrolysis test under N₂ gas flow, as shown in Figure 1a, using a vertical tube furnace as the heating source.

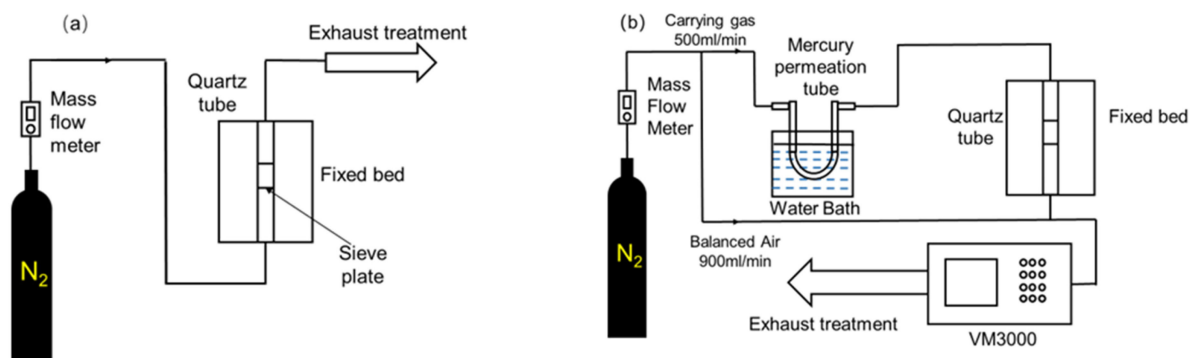


Figure 1. Test system diagram. (a) Fixed-bed biochar preparation system. (b) Fixed-bed mercury adsorption test system.

A fixed-bed mercury adsorption test system was used to study the mercury removal performance of the sample, as shown in Figure 1b. Elemental mercury is produced in the mercury permeation tube in the water bath. The VM3000 mercury vapor analyzer produced by MI company in Germany was used to monitor the mercury concentration in real-time, with the initial mercury concentration set at 100 µg/m³. A tubular furnace was used to simulate a fixed bed and adjust the test temperature. As the inlet volume of the VM3000 mercury vapor analyzer was 1.4 L/min, the flow rate of the demercury carrier gas N₂ was set at 500 mL/min, and 900 mL/min N₂ was introduced into the bypass as the equilibrium gas.

2.4. Sample Preparation

2.4.1. Preparation of Modified Biochar

Walnut shell biochar (FeCeCu/BC) modified by 10%Fe-4%Ce-2%Cu was prepared by a sol-gel combined with co-precipitation method. Walnut shells were ground and sieved to obtain walnut shell biomass with a particle size of 250 mesh (58–75 µm), a weight of 15 g biomass, 8.643 g FeCl₃·6H₂O, 2.214 g Ce(NO₃)₃·6H₂O and 1.403 g CuSO₄·5H₂O. The mass of the metal compound is obtained from Equation (1):

$$m_{\text{compound}} = \frac{15}{0.84} \times A\% \times \frac{M_{\text{compound}}}{M_A} \quad (1)$$

where m_{compound} is the compound mass of required element A, $A\%$ is the doping mass ratio of element A and M_A and M_{compound} are the molar masses of element A and the compound of A, respectively.

The above biomass and metal compounds were dissolved in a mixed solution of 100 mL anhydrous ethanol and 20 mL deionized water and stirred well. Then, 15 mL 1,2 epichlorohydrin and 1 mL DMF were added to form a sol, and after heating in a water bath at 40 °C for 24 h, 2.7 mL ethyl orthosilicate mixed with 0.7 mL anhydrous ethanol was added to the sol to disperse the sol as a wet gel. The precursor material (FeCeCu/precursor) was obtained by heating it in a water bath at 60 °C for 24 h and then drying and grinding at 90 °C. FeCeCu/precursor (6–7 g) was weighed and heated at 600 °C for 10 min under N₂ airflow with a flow rate of 200 mL/min to obtain FeCeCu/BC. In addition, unmodified BC was obtained by pyrolysis of 250 mesh walnut shell biomass under the same conditions.

2.4.2. Preparation of Mg-MOF-74

Mg-MOF-74 was prepared by the solvothermal method with slight modifications: 2.5 mmol $\text{Mg}(\text{NO}_3)_2 \cdot 6\text{H}_2\text{O}$ and 0.8 mmol H_4DOBDC were weighed and dissolved in 60 mL DMF, 4 mL deionized water and 4 mL EtOH mixed solution and stirred magnetically for 30 min until the solution was clear and transparent to obtain the Mg-MOF-74 precursor solution. The precursor solution was transferred to a hydrothermal synthesis reactor with a 100 mL polytetrafluoroethylene lining, heated at 125 °C for 24 h and then naturally cooled to room temperature. The product was placed in a beaker with an appropriate amount of DMF, stirred for 1 h and then left to remove the unreacted solute. The supernatant was filtered out and stirred with new DMF every 12 h, repeated 3–4 times and then dried at 125 °C. The yellow Mg-MOF-74 powder was obtained after grinding, and was recorded as Mg-MOF-74(1), with a yield of 0.2 g and 90%.

To explore whether Mg-MOF-74 can be mass-produced by the solvothermal method, the solvent volume and mass–liquid ratio of the precursor solution were changed under the same preparation conditions. As shown in Table 1, the yields of the final products were all approximately 90%.

Table 1. Mg-MOF-74 prepared with different solvent volumes and mass liquid ratios.

Samples	Molar Ratio of Solute ($\text{Mg}(\text{NO}_3)_2 \cdot 6\text{H}_2\text{O}$: H_4DOBDC)/mmol	Volume Ratio of Solvent (DMF: Deionized Water: EtOH)/mL	Volume of Polytetrafluoroethylene Lining/mL
Mg-MOF-74(1)	2.5:0.8	60:4:4	100
Mg-MOF-74(2)	5:1.6	120:8:8	200
Mg-MOF-74(2.5)	6.25:2	150:10:10	250
Mg-MOF-74(6:2)	6:2	120:8:8	200
Mg-MOF-74(12:4)	12:4	120:8:8	200
Mg-MOF-74(15:5)	15:5	120:8:8	200
Mg-MOF-74(18:6)	18:6	120:8:8	200
Mg-MOF-74(1)	2.5:0.8	60:4:4	100

The XRD and SEM characterization results of Mg-MOF-74 samples under different preparation conditions are shown in Figures 2 and 3, respectively. It was found that the XRD characterization results of all samples were roughly similar, and the characteristic peak of Mg-MOF-74 appeared in the vicinity of $2\theta = 6.9^\circ$ and 11.9° [13], which indicated that Mg-MOF-74 was successfully synthesized. When the mass-to-liquid ratio was constant with increasing solvent volume, the characteristic peak of the sample slightly shifted to a low angle, and the peak intensity also decreased. When the mass-to-liquid ratio increased, the characteristic peak of the sample shifted to a lower angle, obviously, the peak intensity decreased significantly and spurious peaks appeared, indicating that the crystallization degree of the sample had gradually deteriorated. Combined with the analysis results of pore structure (as shown in Table 2), it can be seen that the increase in solvent volume and mass-to-liquid ratio led to the deterioration of the pore structure of the Mg-MOF-74 obtained, mainly in terms of the decrease in specific surface area and pore volume, among which the influence of the mass-to-liquid ratio is more obvious. The results also show that Mg-MOF-74 synthesized by the solvothermal method can only be used for small-batch preparation but is not suitable for large-batch production. Combined with the characterization results, the Mg-MOF-74(1) sample was used as the raw material for the preparation of MOF-based composites.

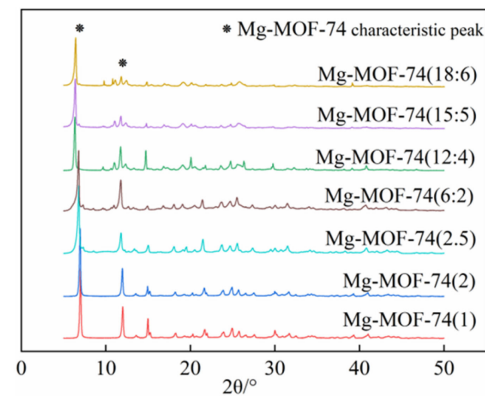


Figure 2. XRD patterns of Mg-MOF-74.

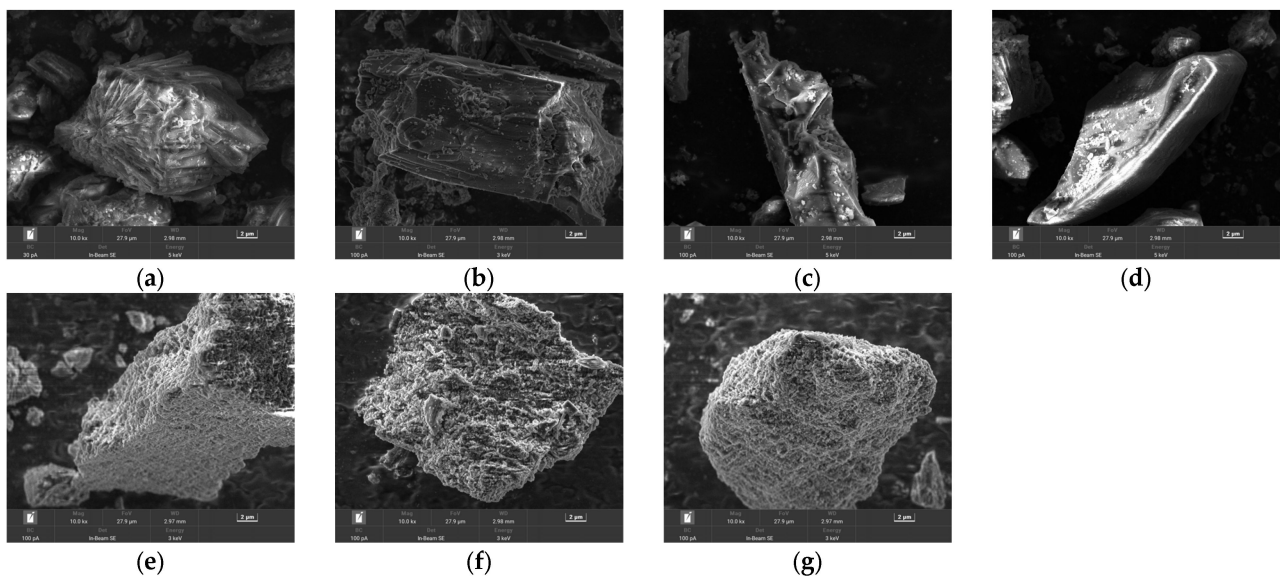


Figure 3. SEM results of Mg-MOF-74. (a) Mg-MOF-74(1). (b) Mg-MOF-74(2). (c) Mg-MOF-74(2.5). (d) Mg-MOF-74(6:2). (e) Mg-MOF-74(12:4). (f) Mg-MOF-74(15:5). (g) Mg-MOF-74(18:6).

Table 2. Pore structure parameters of Mg-MOF-74.

Samples	Specific Surface Area of BET/(m ² .g ⁻¹)	Pore Volume/(cm ³ .g ⁻¹)	Average Pore Diameter/(m ² .g ⁻¹)
Mg-MOF-74(1)	187.0287	0.1363	2.9142
Mg-MOF-74(2)	184.2882	0.1339	2.9336
Mg-MOF-74(2.5)	179.0822	0.1298	2.9637
Mg-MOF-74(6:2)	120.9055	0.1072	3.3503
Mg-MOF-74(12:4)	55.7503	0.0371	4.0793
Mg-MOF-74(15:5)	37.0171	0.0257	4.2643
Mg-MOF-74(18:6)	22.0524	0.0077	4.6327

2.4.3. Preparation of Mg-MOF-74 and FeCeCu/BC Composites

According to the synthesis methods of MOF composites in references [14,15], combined with the microscopic characteristics of Mg-MOF-74 and biochar, three composite preparation methods were proposed: co-pyrolysis method, sol-gel method and in situ growth method. As the co-pyrolysis method involved the physical mixing of Mg-MOF-74 and FeCeCu/BC, the physical mixing method was also studied as a composite method. The microscopic morphology of all the MOF-based composites synthesized through different methods is shown in Figure 4.

1. Physical mixing method: the produced Mg-MOF-74 and FeCeCu/BC were mixed and ground for 10 min at a ratio of 1:1 by mass. The obtained samples are denoted as MgMOF/mixed;
2. Co-pyrolysis method: Mg-MOF-74 was mixed with FeCeCu/BC and FeCeCu/precursor in a ratio of 1:1, ground for 10 min, and then heated at 600 °C for 10 min in a N₂ flow of 200 mL/min. The obtained samples are denoted as MgMOF/BC and MgMOF/precursor, respectively. In addition, to better investigate the properties and physicochemical properties of the products obtained by co-pyrolysis, the pyrolysis products of Mg-MOF-74 were characterized and tested, and the samples are denoted as MgMOF/pyrolysis;
3. Sol-gel method: Combined with the preparation process of biochar, Mg-MOF-74 was put into the mixed solution and stirred well before adding 1,2-epichlorohydrin. The samples are denoted as MgMOF/sol-gel according to the preparation process for biochar. Because of the yield of Mg-MOF-74, the mass ratio of Mg-MOF-74 to biomass was 1:5;
4. In situ growth method: FeCeCu/BC was added to the Mg-MOF-74 precursor solution at a ratio of Mg-MOF-74: FeCeCu/BC = 1:1 and stirred for 30 min. The solution was placed in the reactor according to the synthesis method of Mg-MOF-74, and the resulting sample was denoted MgMOF/in situ growth.

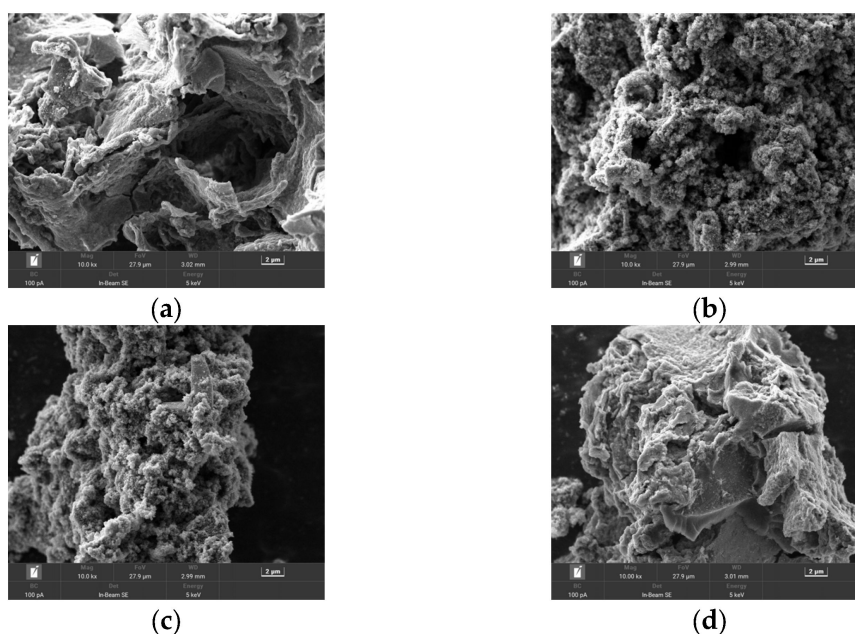


Figure 4. SEM results of Mg-MOF-74 composites. (a) Physical mixing method. (b) Co-pyrolysis method. (c) Sol-gel method. (d) In situ growth method.

3. Results

3.1. Mercury Removal Performance

The cumulative mercury adsorption amount q per unit mass sample is used as the research index of mercury removal performance, and the calculation formula is as follows:

$$q = \frac{F}{m} \sum_0^t C_{in} - C_{out} \quad (2)$$

where q is the cumulative mercury adsorption amount, ng/g; F is the flow rate, L/s; m is the sample mass, g; the dosage in the test is 0.1 g; and C_{in} and C_{out} are the inlet mercury concentration and the outlet mercury concentration, ng/L, respectively.

The samples prepared above were tested for mercury removal. The test time was when the samples reached adsorption saturation (the outlet concentration no longer increased and reached more than 95% of the inlet concentration), or 3 h. The cumulative adsorption amount curve of the samples at an adsorption temperature of 50 °C is shown in Figure 5. Mg-MOF-74 (682.73 ng/g), MgMOF/pyrolysis (1124.10 ng/g) and unmodified BC (4825.10 ng/g) reached adsorption saturation in a relatively short period of time, which showed that the mercury removal performance of these samples was poor. Fe-CeCu/BC (138,114.59 ng/g), after a metal doping modification, greatly improved the performance of mercury removal compared to unmodified biochar. For the composites, MgMOF/mixed (57,863.96 ng/g), MgMOF/precursor (84,746.76 ng/g) and MgMOF/in situ growth (102,196.17 ng/g) greatly improved performance compared to Mg-MOF-74 for mercury removal, but none of them reached the adsorption amount of FeCeCu/BC. While the cumulative adsorption amount of MgMOF/BC (139,378.96 ng/g) was slightly higher than that of FeCeCu/BC, the MgMOF/sol-gel showed a larger increase than that of FeCeCu/BC, corresponding to a cumulative adsorption amount of 180,686.52 ng/g.

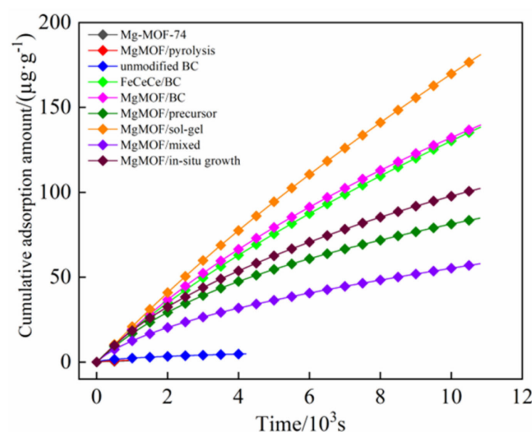


Figure 5. Cumulative mercury adsorption of 50 °C.

The influence of the adsorption temperature on the cumulative adsorption amount of the sample is shown in Figure 6. It was found that the performance of the samples formed by different composite methods for mercury removal was not fixed by the adsorption temperature. Among them, the adsorption amount of the unmodified BC and FeCeCu/BC increased slightly with increasing temperatures, but the change was not significant. For MgMOF/in situ growth, the mercury removal performance of MgMOF/in situ growth decreased sharply with increasing temperature. With increasing temperature, the mercury removal performance of MgMOF/mixed and MgMOF/precursor samples first increased and then decreased, and the adsorption amount of both samples was lower than that of FeCeCu/BC. The mercury removal performance of MgMOF/sol-gel decreased slightly with increasing temperature. The mercury removal performance of the MgMOF/BC sample can obviously be improved with increasing temperature, and both had higher adsorption amounts than FeCeCu/BC, which had better mercury removal performance.

3.2. Pyrolysis Characteristics

To investigate the composite preparation process of co-pyrolysis and sol-gel method and the corresponding structure-activity relationships, Mg-MOF-74, FeCeCu/BC, FeCeCu/precursor, Mg-MOF-74 and FeCeCu/precursor grinding and mixing (Mg-MOF-74 + precursor, which is MgMOF/precursor after pyrolysis), MgMOF/precursor of sol-gel and MgMOF/mixed (MgMOF/BC after pyrolysis) were subjected to thermogravimetric tests with a heating rate of 10 °C/min under N₂ atmosphere, and the weight loss characteristics obtained are shown in Figure 7.

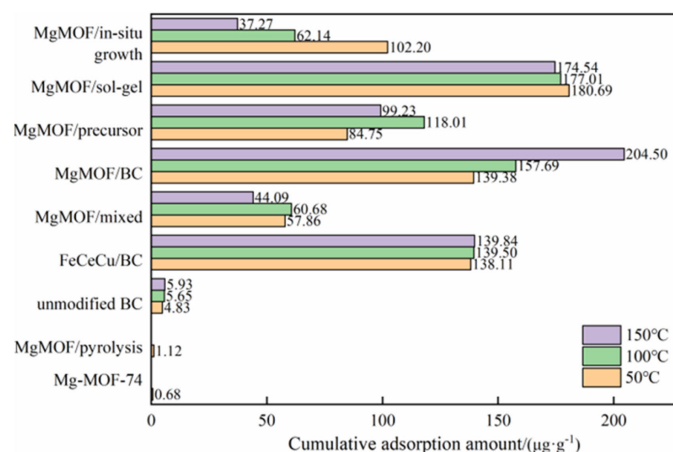


Figure 6. Effect of adsorption temperature on mercury removal performance.

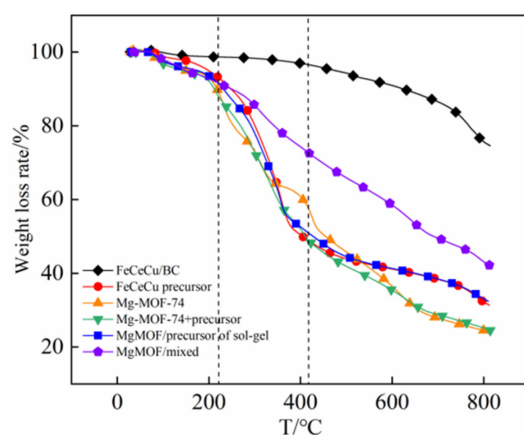


Figure 7. Thermogravimetric curves of Mg-MOF-74 composite.

Since FeCeCu/BC is the product of pyrolysis at 600 °C, the weight loss rate is low before 600 °C, and rapid weight loss does not start until near 800 °C. The weight loss of Mg-MOF-74 mainly consists of three weight loss stages. The first stage is from room temperature to 220 °C, which is mainly the volatilization of residual solvent molecules. The second stage is at 220–420 °C, mainly due to the shedding of organic ligand side chain molecules and the partial collapse of the skeleton. The third stage is after 420 °C, with the collapse of the skeleton. The molecular structure of Mg-MOF-74 is destroyed, forming a MgO-porous carbon structure [16]. The weight loss curve of MgMOF/mixed basically overlaps with that of Mg-MOF-74 before 220 °C and is between those of FeCeCu/BC and Mg-MOF-74 after 220 °C, but the weight loss rate is almost constant. There is no change in the weight loss rate similar to that of Mg-MOF-74 at approximately 400 °C, indicating that grinding makes FeCeCu/BC and Mg-MOF-74 mix homogeneously and makes the two interact during pyrolysis, which in turn affects the pyrolysis process. The weight loss of FeCeCu/precursor can also be divided into three weight loss stages. The first stage is from room temperature to 220 °C, including the volatilization of solvent molecules and a small amount of internal cross-linking, depolymerization, a hydrogen bond-breaking reaction and the release of light gases. From 220 °C to 420 °C, the rapid weight loss is caused by the intense pyrolysis of hemicellulose and lignocellulose and the volatilization of volatile compounds such as tar. After 420 °C, the residues slowly pyrolyze and carbonize to form porous FeCeCu/BC. The weight loss curve of the MgMOF/sol-gel precursor basically overlaps with that of Mg-MOF-74 in the first stage and with that of the FeCeCu/precursor in the second and third stages, with a change in weight loss rate similar to that of Mg-MOF-74 near 400 °C. This is because the addition of Mg-MOF-74 affects the weight loss rate. The

effect is small because of the relatively small doping amount. The weight loss curve of Mg-MOF-74 + precursor is clearly distinguished in three stages. The weight loss rate of each stage changes little, and the curve is smoother. The weight loss rate of pyrolysis near 350 °C and 500–600 °C is greater than that of pyrolysis alone. The other temperature ranges are between the pyrolysis curves of the two substances alone, indicating that the mixture of Mg-MOF-74 and FeCeCu/precursor at a 1:1 ratio causes an obvious interaction between them during co-pyrolysis and affects the process of co-pyrolysis.

According to the thermogravimetric results, it can be speculated that the mechanism of preparing composite materials by co-pyrolysis and the sol–gel method, both of which interact during pyrolysis, results in a composite reaction between materials. The chemical composition of the resulting composite should be a composite product of the MgO-porous carbon structure with FeCeCu/BC, which can be verified by subsequent characterization. Grinding itself can allow the two samples to be mixed evenly or even undergo compounding. Because the in situ growth method does not involve the pyrolysis process, a thermogravimetric test was not carried out.

3.3. Pore Structure

The pore structure parameters of the samples are shown in Table 3. The FeCeCu/BC, MgMOF/sol–gel and MgMOF/BC samples with good mercury removal performance have similar average pore sizes and larger pore volumes, and the proportion of mesopores is higher than that of micropores, indicating that the average pore size and pore volume have a greater influence on the performance of mercury removal. The pore volumes of MgMOF/mixed, MgMOF/in situ growth and MgMOF/precursor are similar. The MgMOF/precursor with a higher pore size and mesopore percentage has better mercury removal performance, indicating that the influence of the pore size is greater. MgMOF/in situ growth has a larger pore volume, but the smallest average pore size has higher adsorption at 50 °C, indicating that pore volume affects the upper limit of mercury removal performance. The specific surface area, pore volume and pore size of unmodified BC are small, so the physical adsorption capacity is weak and the mercury removal performance is poor. The specific surface area and pore volume of Mg-MOF-74 and MgMOF/pyrolysis are larger, but the mercury removal performance is worse, which means that the mercury removal performance is affected not only by physical adsorption but also by chemical adsorption and catalytic oxidation. Therefore, for the FeCeCu/BC and Mg-MOF-74 composites, the mercury removal performance is affected by the combined effects of physical adsorption, chemical adsorption and catalytic oxidation. In addition, the higher the pore volume, the higher the upper limit of its mercury removal performance. The proper pore diameter is beneficial to physical adsorption.

Table 3. Pore structure parameters of the samples.

Samples	Specific Surface Area of BET/(m ² ·g ^{−1})	Pore Volume/(cm ³ ·g ^{−1})	Average Pore Diameter/nm	Relative Pore Volume/%		
				Micropore	Mesopore	Macropore
unmodified BC	39.2144	0.0284	3.1916	29.22	68.66	2.12
Mg-MOF-74	187.0287	0.1363	2.9142	36.59	63.39	0.02
MgMOF/pyrolysis	225.2365	0.3025	5.3730	23.86	75.67	0.47
FeCeCu/BC	107.7644	0.1125	4.1747	30.24	68.68	1.08
MgMOF/mixed	119.6446	0.1178	3.4478	33.42	65.89	0.69
MgMOF/in situ growth	138.8870	0.1188	3.4228	34.91	64.74	0.35
MgMOF/sol–gel	113.6318	0.1304	4.5888	25.84	67.28	6.88
MgMOF/precursor	128.6591	0.1177	5.5022	18.89	79.45	1.66
MgMOF/BC	207.4954	0.2150	4.1442	14.28	85.06	0.66

3.4. Crystal Phase Structure

To investigate the crystalline phase structure of the fabricated materials, XRD characterization analysis was performed. The results are shown in Figure 8. The XRD diagram of

unmodified BC shows a typical amorphous graphite structure. The graphitization degree of FeCeCu/BC modified by iron metal decreases, and metal oxides and solid solutions such as FeCu_4 , Fe_2O_3 , Cu_2O , CuO , Fe_3O_4 , CeO_2 , Ce_2O_3 , CuFeO_2 and CeFeO_3 appear on the surface. These substances can increase the chemical adsorption sites of biochar and improve its chemical adsorption capacity. Part of the elemental mercury can be oxidized, so the mercury removal performance of FeCeCu/BC is greatly improved compared with that of unmodified BC [17]. The XRD diagram of MgMOF/pyrolysis shows only the peak of MgO with low intensity, indicating that the pyrolysis product of Mg-MOF-74 is a MgO-porous carbon structure, which is consistent with the thermogravimetric results [18]. The XRD diagrams of MgMOF/BC, MgMOF/precursor and MgMOF/sol-gel show that the graphitization degree is further reduced and the peak of MgO appears. The peak strength of the metal oxide and solid solution decreases or even disappears, which shows that the composites are prepared by co-pyrolysis and the sol-gel method. Since both the co-pyrolysis method and the sol-gel method have pyrolysis steps, the addition of Mg-MOF-74 leads to interaction during pyrolysis, which affects the formation of metal oxides and solid solutions, resulting in more metal elements in the amorphous form. The characteristic peak of Mg-MOF-74 also appears in the MgMOF/precursor. The reason is that part of the heat carried by the volatile fraction can protect part of Mg-MOF-74 from destruction, which verifies the previous research results. The XRD results of the samples prepared by the in situ growth method are almost the same as those of Mg-MOF-74. The structure of MgMOF/in situ growth shows that the small molecule Mg-MOF-74 grows on the surface of the large molecule FeCeCu/BC and forms a core-shell structure. In the XRD results of MgMOF/mixed, a solid solution peak with low intensity and some spurious peaks appear. This shows that physical grinding and mixing can make Mg-MOF-74 attach to the surface of FeCeCu/BC, which indicates that there are growth sites of MgMOF-74 on the surface of biochar. Therefore, Mg-MOF-74 composites can also be prepared by in situ growth and physical mixing. This proves once again that the mercury removal performance of FeCeCu/BC and Mg-MOF-74 composites is the result of the combined effects of physical adsorption, chemical adsorption and oxidation.

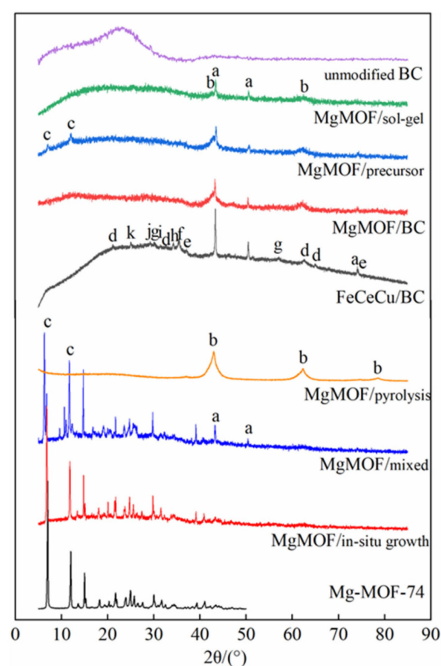


Figure 8. XRD diagram of Mg-MOF-74 composite (a, FeCu_4 ; b, MgO; c, Mg-MOF-74; d, Fe_2O_3 ; e, Cu_2O ; f, CuO ; g, Fe_3O_4 ; h, CeO_2 ; i, Ce_2O_3 ; j, CuFeO_2 ; k, CeFeO_3).

3.5. Surface Chemical Characterization

To investigate the surface functional groups and chemical bonding of the fabricated materials, FTIR characterization analysis was performed, and the results are shown in Figure 9. The unmodified BC mainly consists of –OH (3415 cm^{-1}), C=O (1586 cm^{-1}) and C–O (1428 cm^{-1}) with small peak intensities and low functional group contents. The iron-based metal doping modification resulted in a significant increase in the content of functional groups [19], and the peaks of –CH₂ ($998, 873\text{ cm}^{-1}$), M–OH (564 cm^{-1}) and metal oxides (454 cm^{-1}) appeared, indicating that the surface chemical properties of FeCeCu/BC were greatly improved and the mercury removal ability was enhanced [20]. The functional groups of Mg-MOF-74 include –OH (3391 cm^{-1}), C=O ($1672, 1582\text{ cm}^{-1}$), C=C (1416 cm^{-1}), benzene ring ($1369, 886, 821\text{ cm}^{-1}$), aromatic ring C–H (1221 cm^{-1}), aromatic ring C–O (1110 cm^{-1}) and M–OH (583 cm^{-1}) [21]. After pyrolysis, a large number of functional groups were destroyed, and only –OH (3391 cm^{-1}), C=O (1582 cm^{-1}) and C=C (1416 cm^{-1}) were retained, but peaks of metal oxides with high intensity (480 cm^{-1}) appeared, indicating the formation of a MgO-porous carbon structure after pyrolysis, which is consistent with the thermogravimetric test and XRD results. Compared with the FTIR curve of FeCeCu/BC, the –OH content of MgMOF/BC decreases because –OH is more easily destroyed by heat. Repyrolysis leads to a decrease in the content of –OH and an increase in the content of C=O and –CH₂ in FeCeCu/BC [22], and the peaks of metal oxides become the highest intensity peaks. The FTIR of MgMOF/precursor and MgMOF/sol-gel are more similar, mainly including peaks of –OH (3415 cm^{-1}), C=O (1586 cm^{-1}), C–O (1428 cm^{-1}), aromatic ring C–H (1213 cm^{-1}), M–OH (564 cm^{-1}) and metal oxide (454 cm^{-1}), as well as a lower-intensity benzene ring peak, which indicates the presence of FeCeCu/BC, MgO-porous carbon structure and part of the undecomposed Mg-MOF-74 in both, while the poor performance of MgMOF/precursor for mercury removal than MgMOF/sol-gel is due to the higher doping of Mg-MOF-74 during the preparation of MgMOF/precursor, which has more influence on the pyrolysis process, and the average pore size becoming larger while the pore volume decreases. The formation of metal active sites is also affected, and the content of highly reactive –CH₂ is lower while the content of aromatic ring C–H increases; these factors affect the performance of mercury removal. The peaks of MgMOF/in situ growth are similar to those of Mg-MOF-74, with a few spurious peaks appearing, which again indicates that the structure of Mg-MOF-74 wrapped around the surface of FeCeCu/BC. The shift in peak position and change in peak intensity of the FTIR diagram of MgMOF/mixed, with a small number of spurious peaks appearing, also indicate that the compounding of Mg-MOF-74 with FeCeCu/BC occurs through physical mixing.

3.6. Adsorption Kinetics and Mechanism of Mercury Removal

Four adsorption kinetic models, including the pseudo-first-order kinetic model, pseudo-second-order kinetic model, intraparticle diffusion model and Elovich model, are used to fit the mercury removal data to investigate the reaction mechanism and determine the rate-controlling steps in the adsorption process [23–25]. Among them, the pseudo-first-order kinetic model and the intraparticle diffusion model mainly study the physical adsorption process, while the pseudo-second-order kinetic model and the Elovich model focus on chemical adsorption [26]. The equations of the four models are shown in Equations (3)–(6), and the fitting results are shown in Tables 4 and 5.

Pseudo-first-order kinetic model:

$$q = q_e \left(1 - e^{-tk_1}\right) \quad (3)$$

Pseudo-second-order kinetic model:

$$q = \frac{F}{m} \sum_0^t C_{in} - C_{out} \quad (4)$$

Intraparticle diffusion model:

$$q = \frac{F}{m} \sum_0^t C_{in} - C_{out} \quad (5)$$

Elovich model:

$$q = \frac{F}{m} \sum_0^t C_{in} - C_{out} \quad (6)$$

where q is the cumulative amount of mercury removed at moment t , ng/g; q_e is the equilibrium adsorption amount, ng/g; t is the adsorption time, s; k_1 is the pseudo-first-order rate constant; k_2 is the pseudo-second-order rate constant; k_{id} is the intraparticle diffusion rate constant; C is the constant related to the thickness of the boundary layer; α is the initial adsorption rate; and β is the constant related to the surface coverage and activation energy, $t_0 = 1/\alpha\beta$.

The fitted correlation coefficients, R^2 , are all close to or exceed 0.99, indicating that all four kinetic models are applicable to the sample mercury removal process, which proves that the removal process capacity of the sample is the result of the combined effects of physical and chemical adsorption, external mass transfer and internal diffusion, and that the elemental mercury adsorption process is related to the adsorption sites of the sample rather than single monolayer adsorption [27]. The R^2 fitted by the pseudo-first-order kinetic model is slightly smaller than that of the pseudo-second-order kinetic model and generally lower than that of the Elovich model, indicating that chemical adsorption has a greater effect on the adsorption rate than physical adsorption. With increasing temperature, the R^2 fitted by the intraparticle diffusion model shows a decreasing or first increasing and then decreasing trend, indicating that the increase in temperature will make the control of the adsorption rate by intraparticle diffusion weaker. For MgMOF/BC and MgMOF/sol-gel, the R^2 fitted by the pseudo-first-order kinetic model, pseudo-second-order kinetic model and Elovich model are all greater than 0.999, indicating that the external mass transfer and physical–chemical adsorption on the surface are strong, which is also consistent with the fact that both are the best composites for mercury removal performance.

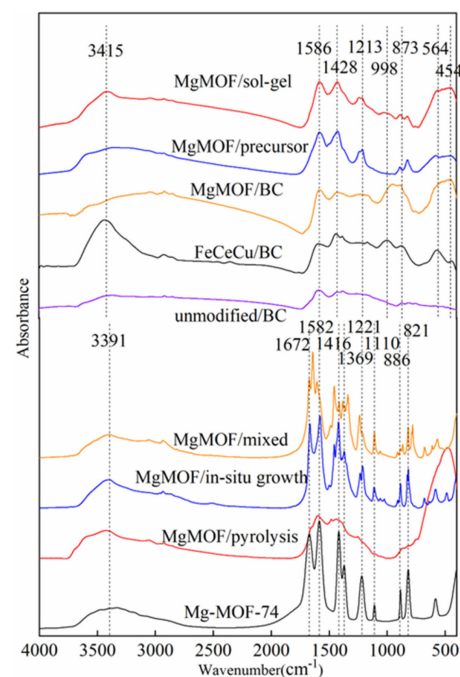


Figure 9. FTIR diagram of Mg-MOF-74 composite.

Table 4. Adsorption kinetic fitting parameters (pseudo-first-order equation and pseudo-second-order equation).

Samples	$T/^\circ\text{C}$	Pseudo-First-Order Kinetic			Pseudo-Second-Order Kinetic		
		R^2	k_1	q_e	R^2	k_2	q_e
unmodified BC	50	0.98790	5.43×10^{-4}	5285.86	0.99258	6.72×10^{-8}	7120.80
	100	0.98754	7.48×10^{-4}	5554.03	0.99504	9.61×10^{-8}	7277.17
	150	0.99489	1.82×10^{-4}	10,724.77	0.99498	6.15×10^{-9}	18,030.50
FeCeCu/BC	50	0.99965	6.97×10^{-5}	258,263.05	0.99976	9.35×10^{-11}	442,928.87
	100	0.99983	6.39×10^{-5}	277,412.99	0.99989	7.74×10^{-11}	482,204.94
	150	0.99978	3.26×10^{-5}	474,071.27	0.99975	1.98×10^{-11}	885,802.46
Mg-MOF-74	50	0.98990	8.90×10^{-4}	1255.53	0.99003	2.94×10^{-7}	1997.09
MgMOF/pyrolysis	50	0.98390	9.00×10^{-4}	2120.93	0.98487	2.08×10^{-7}	3158.84
MgMOF/mixed	50	0.99505	1.59×10^{-4}	68,256.11	0.99679	1.16×10^{-9}	100,816.32
	100	0.99408	1.57×10^{-4}	71,872.43	0.99588	1.09×10^{-9}	106,144.32
	150	0.99726	9.13×10^{-5}	68,757.25	0.99761	5.17×10^{-10}	112,141.92
MgMOF/BC	50	0.99984	8.39×10^{-5}	232,080.53	0.99994	1.32×10^{-10}	388,775.95
	100	0.99969	9.97×10^{-5}	194,515.98	0.99989	1.99×10^{-10}	317,481.19
	150	1.00000	2.73×10^{-5}	799,582.79	1.00000	9.74×10^{-12}	1,499,826.4
MgMOF/precursor	50	0.99799	1.60×10^{-4}	100,639.32	0.99919	7.80×10^{-10}	149,692.53
	100	0.99951	1.08×10^{-4}	169,029.49	0.99980	2.59×10^{-10}	271,376.11
	150	0.99992	1.45×10^{-4}	124,734.99	0.99993	5.26×10^{-10}	191,097.60
MgMOF/sol-gel	50	0.99995	4.60×10^{-5}	459,113.49	0.99997	3.12×10^{-11}	827,144.38
	100	0.99999	5.49×10^{-5}	394,543.07	1.00000	4.47×10^{-11}	700,221.44
	150	0.99999	4.49×10^{-5}	454,790.48	0.99999	3.04×10^{-11}	823,359.45
MgMOF/in situ growth	50	0.99849	1.29×10^{-4}	133,444.20	0.99917	4.28×10^{-10}	206,663.41
	100	0.99846	2.75×10^{-4}	64,027.57	0.99997	2.81×10^{-9}	85,988.20
	150	0.99392	7.34×10^{-5}	67,044.38	0.99398	4.04×10^{-10}	111,909.96

Combining the adsorption kinetics with the sample characterization results, the mechanism of mercury removal from the samples can be speculated. Mg-MOF-74 and Mg-MOF/pyrolysis have larger specific surface areas and pore volumes, but the pore channels are mainly one-dimensional pores [28]. The pore size is not conducive to the capture of mercury, and the lack of chemical adsorption sites for mercury results in poor mercury removal performance. The performance of unmodified BC is also poor due to its small pore size and low pore volume. The temperature increase has a small effect on the performance of unmodified BC, indicating the presence of a small number of chemical adsorption sites on its surface [29]. The metal-doped modified biochar FeCeCu/BC has a good pore structure, abundant metal active sites and surface functional groups and a good physical and chemical adsorption effect on elemental mercury and the ability to oxidize elemental mercury [30]. Based on the adsorption kinetic fitting, it is also evident that the performance of FeCeCu/BC for mercury removal is a combination of physicochemical adsorption and internal-external mass transfer. The mechanism of mercury removal with Mg-MOF-74 composites is based on FeCeCu/BC, and the composite can change the pore structure, crystalline phase structure and surface functional group content, as well as the physicochemical adsorption properties of the material [31]. The composite obtained by physical mixing and the in situ growth method has a structure of Mg-MOF-74 wrapped or attached to the surface of FeCeCu/BC. In the process of mercury removal, the elemental mercury contacts Mg-MOF-74 on the surface first and then diffuses into the modified biochar. Therefore, although the composite increases the pore volume of the sample, the pores of Mg-MOF-74 are not suitable for mercury removal, so instead, it affects the external mass transfer and internal diffusion to make the physical adsorption performance worse, which affects the overall performance of mercury removal. The composites prepared by co-pyrolysis and the

sol-gel method are composed of composite products of the MgO-porous carbon structure and FeCeCu/BC, and a small amount of incomplete pyrolysis of Mg-MOF-74 exists, which changes the pore structure. The co-pyrolysis of the material with the precursor also affects the pyrolysis process and the surface properties and metal fugitive morphology of the product, in which the pore structure of MgMOF/BC becomes better and the chemical properties of FeCeCu/BC are basically preserved with little effect on chemical adsorption, so the performance of mercury removal is improved and more obvious with increasing temperature. The MgMOF/precursor is promoted by the pyrolysis process due to co-pyrolysis, and although the pore volume is improved, the pore size becomes larger and the surface properties become worse, which in turn worsens the removal of mercury. The Mg-MOF-74 doping in MgMOF/sol-gel is small. The pore volume is improved, and the pore size does not change significantly. The chemical properties are less affected, and the mercury removal performance is improved.

Table 5. Fitting parameters of adsorption kinetics (intra-particle diffusion and Elovich kinetic).

Samples	T/°C	Intra-Particle Diffusion			Elovich Kinetic		
		R ²	k _{id}	q _e	R ²	α	β
unmodified BC	50	0.99883	75.61	−51.82	0.99670	0.2295	2.07 × 10 ^{−3}
	100	0.99100	88.08	89.01	0.99940	0.1466	3.33 × 10 ^{−3}
	150	0.97473	101.46	−1116.65	0.99511	0.4852	2.78 × 10 ^{−4}
FeCeCu/BC	50	0.98560	1577.60	−32,275.03	0.99985	0.0534	9.99 × 10 ^{−5}
	100	0.98410	1600.49	−33,667.80	0.99994	0.0546	8.84 × 10 ^{−5}
	150	0.97677	1656.49	−40,509.49	0.99972	0.0643	3.76 × 10 ^{−5}
Mg-MOF-74	50	0.97729	26.65	−123.17	0.99033	0.8050	1.63 × 10 ^{−3}
MgMOF/pyrolysis	50	0.98704	44.46	−169.24	0.98642	0.4299	2.12 × 10 ^{−3}
MgMOF/mixed	50	0.99879	616.44	−6866.30	0.99831	0.0757	3.79 × 10 ^{−4}
	100	0.99850	643.63	−7092.67	0.99757	0.0727	3.75 × 10 ^{−4}
	150	0.98730	485.08	−8339.34	0.99798	0.1475	1.53 × 10 ^{−4}
MgMOF/BC	50	0.99011	1606.39	−31,671.54	0.99999	0.0487	1.28 × 10 ^{−4}
	100	0.99290	1481.27	−27,048.81	0.99999	0.0479	1.65 × 10 ^{−4}
	150	0.97306	2401.48	−58,780.47	1.00000	0.0455	3.13 × 10 ^{−5}
MgMOF/precursor	50	0.99876	928.47	−11,411.56	0.99987	0.0517	3.68 × 10 ^{−4}
	100	0.99443	1340.87	−23,370.47	0.99997	0.0501	1.89 × 10 ^{−4}
	150	0.99639	1133.20	−16,864.91	0.99947	0.0483	2.95 × 10 ^{−4}
MgMOF/sol-gel	50	0.97966	2099.52	−47,885.09	0.99998	0.0465	5.80 × 10 ^{−5}
	100	0.98250	2059.07	−45,657.30	0.99999	0.0451	7.19 × 10 ^{−5}
	150	0.97914	2045.58	−47,093.91	0.99998	0.0482	5.59 × 10 ^{−5}
MgMOF/in situ growth	50	0.99690	1138.58	−17,082.39	0.99967	0.0510	2.56 × 10 ^{−4}
	100	0.98204	652.19	−1500.88	0.99792	0.0383	1.03 × 10 ^{−3}
	150	0.97535	406.23	−7070.69	0.99410	0.1914	1.15 × 10 ^{−4}

4. Conclusions

1. Mg-MOF-74 was prepared by the solvothermal method, and the effect of changing the solvent volume and mass-to-liquid ratio on the preparation was investigated. The solvothermal method is only applicable to the preparation of Mg-MOF-74 in small batches, and increasing the solvent volume and mass-to-liquid ratio during preparation will deteriorate the crystallization and pore structure of Mg-MOF-74;
2. Fe-based metal-doped modified walnut shell biochar FeCeCu/BC was prepared using a sol-gel combined with the co-precipitation method. Various composites of Mg-MOF-74 and FeCeCu/BC were prepared by using physical mixing, co-pyrolysis, sol-gel and in situ growth methods, and mercury removal tests were conducted to compare their mercury removal performance. The results show that MgMOF/sol-gel prepared

- by the sol–gel method and MgMOF/BC prepared by the co-pyrolysis method have the best performance of mercury removal, with the highest improvement of 31% and 46% compared to FeCeCu/BC, respectively, indicating that the Mg-MOF-74 composites prepared by suitable composite methods can improve the performance of mercury removal;
3. Thermogravimetric tests, BET, XRD, FTIR characterization analysis and adsorption kinetic fitting were conducted to analyze the composite process and the mechanism of mercury removal from the composites, and the results show that the mercury removal performance of the samples is the result of the combined effect of physical and chemical adsorption. Mg-MOF-74 and MgMOF/pyrolysis are not suitable for mercury removal. The mercury removal of the composites depends on the chemisorption and oxidation of the metal active sites of FeCeCu/BC, and the composite of Mg-MOF-74 and FeCeCu/BC leads to changes in the pore structure and surface properties of the composites, which affect the performance of mercury removal. Physical mixing and in situ growth are Mg-MOF-74 wrapped or attached to the FeCeCu/BC surface, which is not conducive to mercury removal, while the co-pyrolysis and sol–gel methods affect both pore structure and surface properties, and MgMOF/precursor deteriorates the performance of mercury removal due to the deterioration of pore size and surface properties, while MgMOF/BC co-pyrolysis and MgMOF/sol–gel improve the pore structure with little change in surface properties and improve the performance of mercury removal;
 4. The effect of the doping ratio of Mg-MOF-74 on the mercury removal performance of the composites needs to be investigated subsequently, and it can be predicted that for the in situ growth method, physical mixing method, Mg-MOF-74 and FeCeCu/precursor co-pyrolysis, decreasing the doping ratio of Mg-MOF-74 will improve the mercury removal performance, while the Mg-MOF-74 and FeCeCu/BC co-pyrolysis and sol–gel method should also have the most favorable Mg-MOF-74 doping ratio for mercury removal;
 5. The high-temperature conditions used for flue gas formation after coal combustion in power plants can be used to calcine the functional iron-based precursor materials prepared by the sol–gel method, resulting in the pyrolysis of biomass to obtain Mg-MOF-74 composite adsorbents. After that, the obtained adsorbent can effectively remove gaseous Hg^0 in a suitable range of low temperatures. Finally, it can be separated and captured by electrostatic precipitators (ESPs) and fabric filters (FFs). This mercury emission reduction process has a very low cost. Moreover, this method does not need to add new equipment and has a simple process that is suitable for the transformation of existing units and is not limited by the coal type and combustion conditions, so as to realize its own recycling based on “demercuration by waste”, which has broad application prospects.

Author Contributions: Conceptualization, Y.Y. and J.L.; data curation, Q.Y. and Y.Z.; formal analysis, Y.W.; funding acquisition, L.J.; investigation, P.C.; methodology, J.L.; resources, J.L.; software, H.N.; supervision, L.J.; visualization, Y.Y.; writing—original draft preparation, Y.Y.; writing—review and editing, P.C. and L.H. All authors have read and agreed to the published version of the manuscript.

Funding: This research was funded by the State Key Laboratory of Power System and Generation Equipment (SKLD21KM16), Fundamental Research Program of Shanxi Province (20210302124449; 202303021212043), and Shanxi Province Science and Technology Innovation Project of Colleges and Universities (2020L0073).

Institutional Review Board Statement: Not applicable.

Informed Consent Statement: Not applicable.

Data Availability Statement: The data that support the findings of this study are available from the corresponding author upon reasonable request.

Conflicts of Interest: The authors declare no conflict of interest.

References

1. Habuer, Z.; Zhou, Y.; Takaoka, M. Time-Series Analysis of Excess Mercury in China. *J. Mater. Cycles Waste Manag.* **2018**, *20*, 1483–1498. [[CrossRef](#)]
2. Zhao, S.; Duan, Y.; Chen, L.; Li, Y.; Yao, T.; Liu, S.; Liu, M.; Lu, J. Study on Emission of Hazardous Trace Elements in a 350 MW Coal-Fired Power Plant. Part 1. Mercury. *Environ. Pollut.* **2017**, *229*, 863–870. [[CrossRef](#)]
3. Tong, Y.; Wang, K.; Gao, J.; Yue, T.; Zuo, P.; Wang, C.; Tong, L.; Zhang, X.; Zhang, Y.; Liang, Q.; et al. Mercury Distribution and Emission Reduction Potentials of Chinese Coal-Fired Industrial Boilers. *Air Qual. Atmos. Health.* **2022**, *15*, 967–978. [[CrossRef](#)]
4. Azmi, N.Z.M.; Buthiyappan, A.; Raman, A.A.A.; Patah, M.F.A.; Sufian, S. Recent Advances in Biomass Based Activated Carbon for Carbon Dioxide—A Review. *J. Ind. Eng. Chem.* **2022**, *116*, 1–20. [[CrossRef](#)]
5. Qi, L.; Wang, X.; Wang, W.; Li, J.; Huang, Y. Mercury Removal from Coal Combustion Flue Gas by Pyrite-Modified Fly Ash Adsorbent. *Environ. Sci. Pollut. Res.* **2022**, *29*, 39228–39238. [[CrossRef](#)]
6. Liu, H.; Yuan, B.; Zhang, B.; Hu, H.; Li, A.; Luo, G.; Yao, H. Removal of Mercury from Flue Gas Using Sewage Sludge-Based Adsorbents. *J. Mater. Cycles Waste Manag.* **2014**, *16*, 101–107. [[CrossRef](#)]
7. Cui, Y.; Huo, Q.; Chen, H.; Chen, S.; Wang, S.; Wang, J.; Chang, L.; Han, L.; Xie, W. Biomass Carbon Magnetic Adsorbent Constructed by One-Step Activation Method for the Removal of Hg⁰ in Flue Gas. *ACS Omega* **2022**, *7*, 9244–9253. [[CrossRef](#)]
8. Jia, L.; Cheng, P.; Yu, Y.; Chen, S.; Wang, C.; He, L.; Nie, H.; Wang, J.; Zhang, J.; Fan, B.; et al. Regeneration Mechanism of a Novel High-Performance Biochar Mercury Adsorbent Directionally Modified by Multimetal Multilayer Loading. *J. Environ. Manag.* **2023**, *326*, 116790. [[CrossRef](#)]
9. Avci, G.; Altintas, C.; Keskin, S. Metal Exchange Boosts the CO₂ Selectivity of Metal Organic Frameworks Having Zn-Oxide Nodes. *J. Phys. Chem. C* **2021**, *125*, 17311–17322. [[CrossRef](#)]
10. Rarotra, S.; Kumar, P.; Satyabrata, S.; Kumar, P.; Kim, K.H. Transformation of Recovered Cobalt from Lithium-Ion Batteries into Zeolitic Imidazolate Framework-67. *J. Mater. Cycles Waste Manag.* **2022**, *24*, 425–432. [[CrossRef](#)]
11. Yang, Y.; Jin, L.; Zhou, L.; Du, X. A Molecular Study of Humid CO₂ Adsorption Capacity by Mg-MOF-74 Surfaces with Ligand Functionalization. *Comput. Mater. Sci.* **2022**, *209*, 111407. [[CrossRef](#)]
12. Flores, G.; Aguilar-Pliego, J.; Martin-Guaregua, N.; Ibarra, I.A.; Sanchez-Sanchez, M. Room-Temperature Prepared Bimetallic Nanocrystalline MOF-74 as Catalysts in the Aerobic Oxidation of Cyclohexene. *Catal. Today* **2022**, *394*, 295–303. [[CrossRef](#)]
13. Kumar, A.; Madden, D.G.; Lusi, M.; Chen, K.-J.; Daniels, E.A.; Curtin, T.; Perry, J.J.; Zaworotko, M.J. Direct Air Capture of CO₂ by Physisorbent Materials. *Angew. Chem. Int. Edit.* **2015**, *54*, 14372–14377. [[CrossRef](#)]
14. Yang, Y.; Li, J.; Dong, Y.; Wang, J.; Cao, L. Preparation of Porous Monoliths via CO₂-in-Water HIPeS Template and the in situ Growth of Metal Organic Frameworks on It for Multiple Applications. *Polym. Adv. Technol.* **2020**, *31*, 1591–1601. [[CrossRef](#)]
15. Moon, H.-S.; Moon, J.-H.; Chun, D.H.; Park, Y.C.; Yun, Y.N.; Sohail, M.; Baek, K.; Kim, H. Synthesis of [Mg-2(DOBDC)(DMF)(2)]@polystyrene Composite and Its Carbon Dioxide Adsorption. *Microporous Mesoporous Mat.* **2016**, *232*, 161–166. [[CrossRef](#)]
16. Lv, Z.; Wang, H.; Chen, C.; Yang, S.; Chen, L.; Alsaedi, A.; Hayat, T. Enhanced Removal of Uranium(VI) from Aqueous Solution by a Novel Mg-MOF-74-Derived Porous MgO/Carbon Adsorbent. *J. Colloid Interface Sci.* **2019**, *537*, A1–A10. [[CrossRef](#)]
17. Jia, L.; Yu, Y.; Li, Z.-P.; Qin, S.-N.; Guo, J.-R.; Zhang, Y.-Q.; Wang, J.-C.; Zhang, J.-C.; Fan, B.-G.; Jin, Y. Study on the Hg⁰ Removal Characteristics and Synergistic Mechanism of Iron-Based Modified Biochar Doped with Multiple Metals. *Bioresour. Technol.* **2021**, *332*, 125086. [[CrossRef](#)]
18. Kang, H.; Shin, J.; Kim, T.-H.; Lee, Y.; Lee, D.; Lee, J.; Kim, G.; Cho, E. Metal-Organic Framework-Derived Magnesium Oxide@Carbon Interlayer for Stable Lithium-Sulfur Batteries. *ACS Sustain. Chem. Eng.* **2023**, *11*, 1344–1354. [[CrossRef](#)]
19. Du, T.; Long, Y.; Tang, Q.; Li, S.; Liu, L. Adsorption Property of Mg-MOF-74 for CO₂/H₂O. *Chem. J. Chin. Univ. Chin.* **2017**, *38*, 225–230. [[CrossRef](#)]
20. Xiao, R.; Gao, T.; Cui, X.; Ji, Y.; Zhang, Y.; Chuai, X.; Xiong, Z.; Liao, Y.; Gu, H.; Yang, J.; et al. Removal of Elemental Mercury from Flue Gas by Recyclable CuCl₂ Modified Magnetospheres Catalyst from Fly Ash: Part 6. Commercial Scale Demonstration at a 1000MWth Coal-Fired Power Plant. *Fuel* **2022**, *310*, 122219. [[CrossRef](#)]
21. Guo, Z.; Zhou, J.; Hou, H.; Wu, X.; Li, Y. Recyclable Mg-MOF-74@cellulose Aerogel Composites for Efficient Removal of Heavy Metals from Wastewater. *J. Solid State Chem.* **2023**, *323*, 124059. [[CrossRef](#)]
22. Wang, F.; Tang, T.; Zhang, R.; Cheng, Z.; Wu, J.; He, P.; Qi, Y.; Chen, S.; Li, W. Magnetically Recyclable CoS-Modified Graphitic Carbon Nitride-Based Materials for Efficient Immobilization of Gaseous Elemental Mercury. *Fuel* **2022**, *326*, 125117. [[CrossRef](#)]
23. Shen, F.; Liu, J.; Wu, D.; Dong, Y.; Zhang, Z. Development of O₂ and NO Co-Doped Porous Carbon as a High Capacity Mercury Sorbent. *Environ. Sci. Technol.* **2019**, *53*, 1725–1731. [[CrossRef](#)]
24. Ma, J.; Yu, F.; Zhou, L.; Jin, L.; Yang, M.; Luan, J.; Tang, Y.; Fan, H.; Yuan, Z.; Chen, J. Enhanced Adsorptive Removal of Methyl Orange and Methylene Blue from Aqueous Solution by Alkali-Activated Multiwalled Carbon Nanotubes. *ACS Appl. Mater. Interfaces* **2012**, *4*, 5749–5760. [[CrossRef](#)]
25. Yang, W.; Liu, Z.; Xu, W.; Liu, Y. Removal of Elemental Mercury from Flue Gas Using Sargassum Chars Modified by NH₄Br Reagent. *Fuel* **2018**, *214*, 196–206. [[CrossRef](#)]
26. Recepoglu, Y.K.; Kabay, N.; Yilmaz-Ipek, I.; Arda, M.; Yoshizuka, K.; Nishihama, S.; Yukel, M. Equilibrium and Kinetic Studies on Lithium Adsorption from Geothermal Water by Lambda-MnO₂. *Solvent Extr. Ion Exch.* **2017**, *35*, 221–231. [[CrossRef](#)]
27. Zhang, Z.; Liu, J.; Wang, Z.; Zhang, J. Bimetallic Fe-Cu-Based Metal-Organic Frameworks as Efficient Adsorbents for Gaseous Elemental Mercury Removal. *Ind. Eng. Chem. Res.* **2021**, *60*, 781–789. [[CrossRef](#)]

28. Majumdar, S.; Tokay, B.; Martin-Gil, V.; Campbell, J.; Castro-Munoz, R.; Ahmad, M.Z.; Fila, V. Mg-MOF-74/Polyvinyl Acetate (PVAc) Mixed Matrix Membranes for CO₂ Separation. *Sep. Purif. Technol.* **2020**, *238*, 116411. [[CrossRef](#)]
29. Zhang, H.; Wang, T.; Sui, Z.; Zhang, Y.; Sun, B.; Pan, W.-P. Enhanced Mercury Removal by Transplanting Sulfur-Containing Functional Groups to Biochar through Plasma. *Fuel* **2019**, *253*, 703–712. [[CrossRef](#)]
30. Qin, S.; Fan, H.; Jia, L.; Jin, Y.; Li, Z.; Fan, B. Molecular Structure Analysis and Mercury Adsorption Mechanism of Iron-Based Modified Biochar. *Energy Fuels* **2022**, *36*, 3184–3200. [[CrossRef](#)]
31. Zhao, H.; Wang, X.; Feng, J.; Chen, Y.; Yang, X.; Gao, S.; Cao, R. Synthesis and Characterization of Zn₂GeO₄/Mg-MOF-74 Composites with Enhanced Photocatalytic Activity for CO₂ Reduction. *Catal. Sci. Technol.* **2018**, *8*, 1288–1295. [[CrossRef](#)]

Disclaimer/Publisher's Note: The statements, opinions and data contained in all publications are solely those of the individual author(s) and contributor(s) and not of MDPI and/or the editor(s). MDPI and/or the editor(s) disclaim responsibility for any injury to people or property resulting from any ideas, methods, instructions or products referred to in the content.